UDC 551.465.755:551.465.557:551.515.21

"BOTTOM STRESS TIME-HISTORY" IN LINEARIZED EQUATIONS OF MOTION FOR STORM SURGES [1]

CHESTER P. JELESNIANSKI [2]

Atlantic Oceanographic and Meteorological Laboratories, ESSA, Miami, Fla.

ABSTRACT

A transient Ekman's transport equation, in which bottom stress is formed as a convoluted integral in terms of surface stress and surface slope, and a continuity equation are used as predictors to compute storm surges in a model basin. Driving forces in the basin are analytically computed, using a model storm to represent actual meteorological conditions.

A coastal boundary condition that relates surface slope to surface stress is developed by balancing slope and drift transports normal to a vertical wall. At interior grid points of the basin, sea-surface heights are computed by numerical means, using the prediction equations. These sea-surface heights are then extrapolated to the coast to agree with the coastal surface slope given by the boundary condition. Coastal storm surges computed in this manner are compared with observed surges to test the model developed in this study.

CONTENTS

1. INTRODUCTION

A mathematical model for storm surges could begin with the theory of drift and slope currents as developed by Ekman (1905, 1923). This theory, though based on simplifying assumptions of shallow-water theory, hydrostatic pressure, homogeneous sea of infinite horizontal extent, constant Coriolis parameter, constant eddy viscosity coefficient, and neglect of lateral stresses and nonlinear interaction terms, is still superbly useful for many investigations. Most of these assumptions are too severe for deep seas of large areal extent where variation of the Coriolis parameter, density stratifications, and lateral stresses are important physical processes. However, the equatious may be of sufficient generality to compute storm surges along shallow continental shelves of limited areal extent where variation of Coriolis parameter is negligible and lateral stress is much smaller than the vertical stress.

Following Ekman, one can write the equation of motion in complex form

$$\frac{\partial w}{\partial t}=-ifw+q+\nu\frac{\partial^2 w}{\partial z'^2} \tag{1}$$

where

$w=u+iv$, horizontal components of current,
f=Coriolis parameter,
$q=-g[(\partial(h-h_0)/\partial x)+i(\partial(h-h_0)/\partial y)]$,
g=gravity,
h=storm surge height,
ν=constant vertical eddy viscosity coefficient,
z'=vertical coordinate positive upward, prime symbol in anticipation of nondimensionalizing, and
h_0=inverse barometric height from atmospheric pressure,

and in a more convenient form to nondimensionalize the vertical coordinate as

$$\left(\frac{\partial}{\partial t}+if\right)w=q+\frac{\nu}{H^2}\frac{\partial^2 w}{\partial z^2} \tag{2}$$

where $z=z'/H$ and $H(x,y)$=depth of the basin.

Ekman's equation (2) is formidable for computational purposes if the vertical coordinate is retained even in a restricted area. However, if the equations are integrated in the vertical to form transport terms and then linearized, considerable simplification in computational procedures is gained. This is justified in storm surge work because currents are only of casual interest compared to the slope or height variations of the sea surface. Equation (2) can then be rewritten as

$$\left(\frac{\partial}{\partial t}+if\right)W=Q+F-\frac{\nu}{H}\frac{\partial w}{\partial z}\bigg|_{z=-1} \tag{3}$$

[1] This study is in partial fulfillment of the requirements for the degree of Doctor of Philosophy of Engineering Science in the School of Engineering and Science of New York University.

[2] Now affiliated with the Techniques Development Laboratory, ESSA, Silver Spring, Md.

where

$$W=H\int_{-1}^{0} wdz,\ Q=Hq,\ \text{and}\ F=(\nu/H)(\partial w/\partial z)|_{z=0}.$$

The vertical coordinate in equation (3) has not yet been completely eliminated. It appears implicitly in the vertical gradient of velocity on the bottom, that is, the bottom stress.[3] By assuming intuitive forms for bottom stress that are not based on Ekman's theory, the vertical coordinate can be eliminated. Such investigations have been carried out by Hansen (1956) and Miyazaki (1965).

Instead of treating bottom stress as an extrapolation of present forces, Platzman (1963) considered the time history of present and past forces using Ekman's theory and derived a *differential* operator for bottom stress in series form. Jelesnianski (1967) used a modification of this scheme in numerical computations of hurricane-generated storm surges along coastal areas. The results appeared to explain some salient features of storm surges.

Platzman's series expansions, designed to act separately on transport and driving forces, had inherent convergence difficulties. The difficulty disappeared only when the two series were truncated to first order for the transport field and zeroth order for the driving forces; thus, the truncated form implies that immediate time-history of forces is sufficient to express bottom stress. This restriction on time history was sufficient motivation for investigating the possibility of using an *integral* operator for bottom stress that incorporates all the time history of the system.

Using Ekman theory, Welander (1957) suggests that bottom stress can be determined from the local time-histories of wind stress and surface slope by means of an integral operator in the form of a convolution integral. In this approach, there is a lag in time between the appearance of wind stress or surface slope and the consequent bottom stress. The operator includes the entire time-history of driving forces indefinitely into the past. Welander also suggests a single prediction equation to compute the surface heights or storm surge, but only his first suggestion is followed in this study. The exact analytical form for bottom stress is approximated by an integral form and computed by numerical techniques. Thus, the transport equation of motion and a continuity equation are used in this prediction scheme.

In Platzman's and Welander's schemes, the vertical coordinate is fully eliminated at the expense of considering a new form for the variation of bottom stress in terms of quantities that are not dependent on the vertical coordinate and time.

Ekman's equation cannot satisfy physical boundary conditions at a wall or coastline, that is, vanishing currents or vanishing current normal to the wall. However, vanishing transports normal to the wall can be used as representative boundary conditions. The case of zero depths at a coastline introduces singularities in the equation of motion that can be treated mathematically and computationally for certain types of depth profiles generally encountered in nature.

It appears from equation (2) that the vertical current profile is a function of driving forces at local points without regard for neighboring points, and similarly the transports in equation (3). This is not true, for we have yet to satisfy the continuity equation

$$\frac{\partial h}{\partial t}=-\frac{\partial U}{\partial x}-\frac{\partial V}{\partial y} \tag{4}$$

where $W=U+iV$ defines the components of the complex transport.

The surface slope ∇h will be called the dynamic slope to distinguish it from the inverted barometer effect. The dynamic slope is treated as a driving force[4] in this study. The driving forces, F and Q in equation (3), have been regarded as independent functions of time, even though they do vary in space and are interdependent. This has been done purely for convenience, but with the understanding that the momentum equation is spatially connected through the continuity equation.

In this study, a model basin and model storm are used with the prediction scheme to compute surges. The computations are performed numerically using finite-difference equations. Comparisons of observed and computed surges are made for three hurricanes that passed Atlantic City with tracks more or less parallel to the coast. The surge from this type of storm passage is very complicated in that several resurgences occur after storm passage, in addition to the peak surge which occurs during storm passage.

2. PREDICTION EQUATIONS IN COMPONENT FORM

For convenience, the momentum equation (3) is now written as

$$\left(\frac{\partial}{\partial t}+if\right)W=Q+F-(\mathcal{C}_Q+\mathcal{C}_F) \tag{5a}$$

where $\mathcal{C}_Q$, $\mathcal{C}_F$ is notation for complex convolution integrals representing bottom stress in terms of surface slope (dynamic and atmospheric pressure) and surface wind stress, respectively. The form of these integrals is given in a later section. In component form, the above becomes

$$\frac{\partial U}{\partial t}=-gH\frac{\partial h}{\partial x}+fV+{}^{(x)}F+gH\frac{\partial h_0}{\partial x}-\sum_{j=1}^{3}\mathcal{C}^{(r_j)}$$

and (5b)

$$\frac{\partial V}{\partial t}=-gH\frac{\partial h}{\partial y}-fU+{}^{(y)}F+gH\frac{\partial h_0}{\partial y}-\sum_{j=1}^{3}\mathcal{C}^{(i_j)}$$

where ${}^{(x)}F$, ${}^{(y)}F$ are components of surface stress. There are six $\mathcal{C}$'s in the above equations, the real (r_j) and imaginary (i_j) part of $\mathcal{C}$ for each of three driving forces, where $j=1$, 2, 3 means dynamic slope or storm surge, slope due to atmospheric pressure, and wind stress driving force, respectively.

[3] In a *stratified* deep sea, it is assumed that the velocity vector vanishes at some distance below the surface because of mass adjustments; thus, bottom stress also vanishes. In this case, lateral stresses are important dissipation forces.

[4] Platzman (1963) treated transport as a driving force in his series expansion, for convenience in numerical computations. His method could equally well treat Q as a driving force.

The surface stress F in this study is given by

$$F=\frac{C\rho_a}{\rho}|V_s|V_s$$

where V_s=complex wind, ρ_a, ρ=air, water density, C the drag coefficient is assumed constant, and $C\rho_a/\rho=3\times10^{-6}$ ft^2/sec^2.

Equation (5b) and the continuity equation (4) are the prediction equations used in this paper. Boundary conditions must be specified to complete the system; these are given in later sections. The numerical scheme for computations is given appendix D.

The numerical scheme was tested; comparisons were made between it and known analytical solutions without bottom stress for resonance phenomena (Reid 1958)—that is, traveling (edge) waves. For comparison purposes, only basins with shallow slopes and *small* coastal depths were used. The computed periods and/or wave lengths agreed with the fundamental mode of the analytically derived dispersion equation to within a few percent. No comparisons were made of the computed amplitudes of the surge since the driving forces of this study are not equivalent to the ones used in known analytic solutions (Greenspan 1956, Munk 1956).

3. BOTTOM STRESS AS A CONVOLUTION INTEGRAL

The bottom stress convolution integral is a mathematical statement that the fluid not only senses present forces but also remembers past forces, that is "time history." For formulating the bottom stress $(\nu/H)(\partial w/\partial z)|_{z=-1}$ in (3), equation (2) is solved for w, the current profile, as an exact convolution integral in terms of the local driving forces F and Q. A boundary condition for the bottom is needed to complete the transport prediction equation; a simple one[5] is $w|_{z=-1}=0$. With this boundary condition, a solution of equation (2) gives bottom stress as

$$\frac{\nu}{H}\frac{\partial w}{\partial z}\bigg|_{z=-1}=\frac{2\nu}{H^2}\left[\int_0^t F(t-\tau)e^{-if\tau}K_F(\tau)d\tau+\int_0^t Q(t-\tau)e^{-if\tau}K_Q(\tau)d\tau\right]$$

(appendix A), where $K_F(\tau)$, $K_Q(\tau)$ are appropriate kernel functions. Note that ν/H^2 can be used as a time scale for the kernel functions; thus, $T_H=(\nu/H^2)t$ is a convenient nondimensional parameter. For large T_H, one form for the kernels is

$$K_F(t)=\sum_{n=0}^{\infty}(-1)^n\pi\left(n+\frac{1}{2}\right)\exp\left\{-\left[\left(n+\frac{1}{2}\right)\pi\right]^2T_H\right\}$$

and (6)

$$K_Q(t)=\sum_{n=0}^{\infty}\exp\left\{-\left[\left(n+\frac{1}{2}\right)\pi\right]^2T_H\right\};$$

and for small T_H, another form is

$$K_F(t)=\frac{1}{\sqrt{\pi}T_H^{3/2}}\sum_{n=0}^{\infty}(-1)^n\left(n+\frac{1}{2}\right)\exp\left[-\frac{\left(n+\frac{1}{2}\right)^2}{T_H}\right]$$

and (7)

$$K_Q(t)=\frac{1}{2\sqrt{\pi T_H}}\left\{1+2\sum_{n=1}^{\infty}(-1)^n\exp\left[-\frac{\left(n+\frac{1}{2}\right)^2}{T_H}\right]\right\}.$$

The characteristic or reference time T_H varies considerably in this study due to variable depths in the basin. Comparisons of the two time scales associated with ν/H^2 and f in the bottom stress convolution integrals suggest the latter time scale to be of small importance in shallow water.

The graphs of the kernels, with T_H as the independent variable, are shown in figure 1. The kernels are uniformly continuous for all positive values except in the neighborhood of $T_H=0$. From equation (7), the structure of the kernels for $T_H\to0+$ (small time or deep water) can be studied, noting that $x^ne^{-x}\to0$ as $x\to\infty$ for all n, $K_Q\to(T_H)^{-1/2}$, and $K_F\to0$ as $T_H\to0+$. The kernel K_F has an essential singularity at $T_H=0$; this is demonstrated by considering the coefficients of a Taylor's expansion of (7) where $d^kK_F/dT_H^k|_{T_H=0}=0$ for $k=0, 1, 2, \ldots$, that is, the power series expansion for K_F vanishes although K_F does not.

Since this study deals with shallow water, the form (6) is preferable to (7). For large values of T_H, $T_H>0.3$, the kernels given by (6) converge rapidly, and only the very first few terms are required in computations; for small T_H, $T_H<0.3$, the series converges very slowly, and many terms would be required. For convenience in numerical computations, either kernel is represented by means of a *finite* series of exponentials consisting of the very first few terms of equation (6) plus correction terms. The kernel can then be written as

$$K\doteq\sum_{n=1}^{N}a_ne^{-b_nt} \tag{8}$$

where N is finite and a_n, b_n are to be specified.

If at each time step in computations the entire convolution integral is recalculated at each surface grid point, an inordinate number of computations and amount of machine core storage are required. By taking advantage of an "exponential" kernel, a recursion formula can be developed to update or modify the integral, using previous values and newly generated data that appear at each time step.

To develop a recursion formula, let G be any of the three driving forces of the convolution integral. Represent its exact kernel by equation (8), then define

$$\mathcal{C}_G(t)=\frac{2\nu}{H^2}\int_0^t G(t-\tau)e^{-if\tau}\sum_{n=1}^{N}a_ne^{-b_n\tau}d\tau. \tag{9}$$

Letting $t=m\Delta t$ and $\mathcal{C}_G(m\Delta t)=\mathcal{C}_G^m$, one can rewrite the

[5] Other bottom boundary conditions may be preferable, such as $(\nu/H)(\partial w/\partial z)|_{z=-1}=sw|_{z=-1}$ or $(\nu/H)(\partial w/\partial z)|_{z=-1}=s|w|w|_{z=-1}$, where s is a slip coefficient. The solutions have forms that are laborious for computations; hence, they are not considered in this preliminary study.

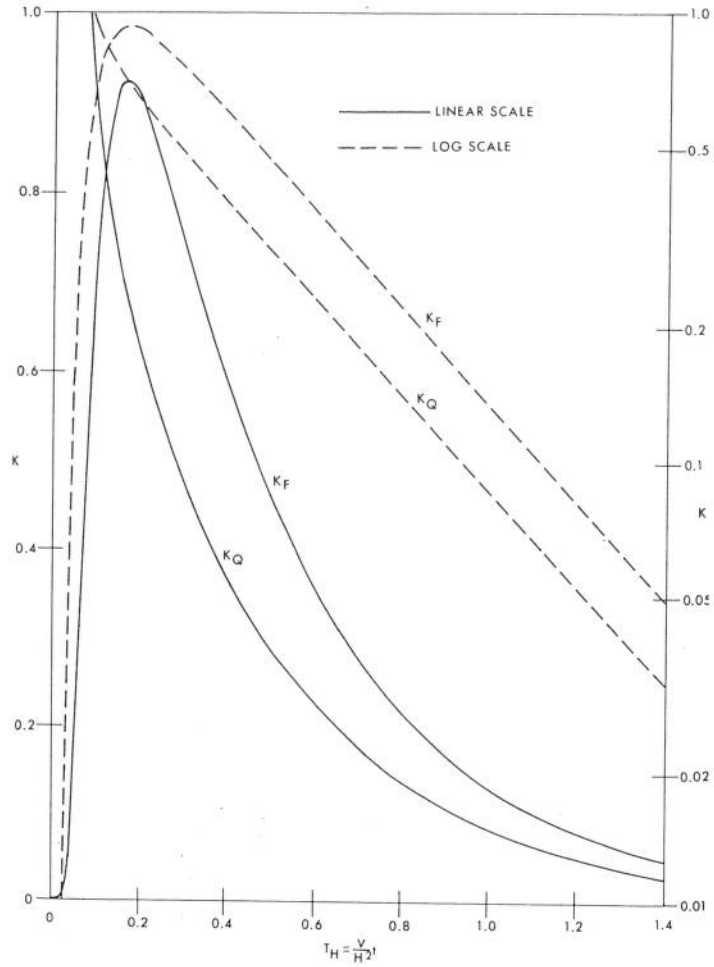

FIGURE 1.—The kernels K_F, K_Q as functions of the nondimensional parameter T_H.

above as

$$\mathcal{C}_G^m=\frac{2\nu}{H^2}\sum_{n=1}^{N} a_n\int_0^{m\Delta t} G(m\Delta t-\tau)e^{-(b_n+if)\tau}d\tau. \quad (10)$$

The summation and integration operators have been interchanged; this is permissible for finite sums. The interchange can also be made for the exact kernels given in equation (6), even though the series are not uniformly convergent at $T_H=0$; the proof of the interchange comes from Lebesgue's theorem as given in appendix B.

Now consider any nth term in equation (10) and form

$$\mathcal{C}_G^m=\frac{2\nu}{H^2}\sum_{n=1}^{N} C_{G_n}^m \quad (11)$$

and

$$C_{G_n}^m=a_n\sum_{k=0}^{m-1}\int_{k\Delta t}^{(k+1)\Delta t} G(m\Delta t-\tau)e^{-(b_n+if)\tau}d\tau. \quad (12)$$

To process (12) into a numerical form, let

$$G(m\Delta t-\tau)\doteq\alpha-(m\Delta t-\tau)\beta \quad (13)$$

where $\alpha=G^{m-k}$, $\beta=[G^{m-k-1}-G^{m-k}]/\Delta t$, and $G'(m\Delta t-\tau)=-\beta$. Here, an assumption is made that the driving forces can be represented by a linear function in the small time interval Δt. Suppose now that equation (12) is integrated by parts. Then

$$C_{G_n}^m=\sum_{k=0}^{m-1}\left[-\frac{a_n}{b_n+if}G(m\Delta t-\tau)e^{-(b_n+if)\tau}\Big|_{k\Delta t}^{(k+1)\Delta t}-\frac{a_n}{b_n+if}\times\int_{k\Delta t}^{(k+1)\Delta t} G'(m\Delta t-\tau)e^{-(b_n+if)\tau}d\tau.\right.$$

Applying (13) to the above equation gives

$$C_{G_n}^m=\sum_{k=0}^{m-1}(A_n)^k[B_nG^{m-k-1}+E_nG^{m-k}] \quad (14)$$

where

$$A_n=e^{-(b_n+if)\Delta t};\ (\quad)^k=k\text{th power};$$

$$B_n=\frac{-a_n}{b_n+if}\left[A_n+\frac{A_n-1}{(b_n+if)\Delta t}\right];\text{ and}$$

$$E_n=\frac{a_n}{b_n+if}\left[1+\frac{A_n-1}{(b_n+if)\Delta t}\right].$$

By suitable contraction on limits in the summation operator, equation (14) can be written as

$$C_{G_n}^m=\gamma_n\sum_{k=1}^{m-1}(A_n)^kG^{m-k}+B_n(A_n)^{m-1}G^0+E_nG^m \quad (15)$$

where $\gamma_n=B_n(A_n)^{-1}+E_n$. In (15), $G^0=0$ since all driving forces are initially zero.

Suppose now that time increases from $m\Delta t$ to $(m+1)\Delta t$. Then

$$C_{G_n}^{m+1}=\gamma_n\sum_{k=1}^{m}(A_n)^kG^{m+1-k}+E_nG^{m+1}, \quad (16)$$

or after some rearrangement

$$C_{G_n}^{m+1}=A_n\left\{\gamma_n\sum_{k=1}^{m-1}(A_n)^kG^{m-k}+E_nG^m\right\}+B_nG^m+E_nG^{m+1}. \quad (17)$$

With the aid of equation (15), the above becomes

$$C_{G_n}^{m+1}=A_nC_{G_n}^m+B_nG^m+E_nG^{m+1}. \quad (18)$$

Returning to equation (11), one obtains

$$\mathcal{C}_G^{m+1}=\frac{2\nu}{H^2}\sum_{n=1}^{N}C_{G_n}^{m+1}=\frac{2\nu}{H^2}\sum_{n=1}^{N}[A_nC_{G_n}^m+B_nG^m+E_nG^{m+1}] \quad (19)$$

which is a simple recursion formula for the convolution integral. Since the convolution integrals are zero at $t=0$, then for initialization $\mathcal{C}_G^0=0$ and $C_{G_n}^0=0$. To break (19) into real and imaginary parts to fit (5b), consider equation (11) at time $t=m\Delta t$. Then

$$\mathcal{C}_{(r_j)}^m+i\mathcal{C}_{(i_j)}^m=\frac{2\nu}{H^2}\sum_{n=1}^{N}[C_{(r_j)n}^m+iC_{(i_j)n}^m],\quad j=1,2,3, \quad (20)$$

where

$$C^m_{(r_j)n}=A_{(r)n}C^{m-1}_{(r_j)n}-A_{(i)n}C^{m-1}_{(i_j)n}+B_{(r)n}G^{m-1}_{(r_j)}-B_{(i)n}G^{m-1}_{(i_j)}+E_{(r)n}G^m_{(r_j)}-E_{(i)n}G^m_{(i_j)}$$

and (21)

$$C^m_{(i_j)n}=A_{(i)n}C^{m-1}_{(r_j)n}+A_{(r)n}C^{m-1}_{(i_j)n}+B_{(i)n}G^{m-1}_{(r_j)}+B_{(r)n}G^{m-1}_{(i_j)}+E_{(i)n}G^m_{(r_j)}+E_{(r)n}G^m_{(i_j)}$$

and where $G_{(r_j)}$, $G_{(i_j)}$ means real and imaginary parts of the jth driving force and the subscripts $(r)n$, $(i)n$ mean real and imaginary parts of the complex coefficients A_n, B_n, and E_n. The complex coefficients given by equation (14), although formidable in appearance, can be computed once and for all when a_n and b_n from (8) are specified for each kernel separately. Note that $j=1$, 2 have the same kernel K_Q, but different driving forces.

4. APPROXIMATING THE KERNELS K_F, K_Q FOR NUMERICAL COMPUTATIONS

It is very difficult to form the kernels K_F, K_Q with great accuracy throughout the positive T_H axis when using the finite sum of exponents given by equation (8). This difficulty arises because of the nonuniform convergence of the kernels at the point $T_H=0$. For shallow water, where bottom stress is most important, the kernels can be adequately represented for moderate to large time intervals with the first term of the series (6); consequently, it is desirable to consider this first term as the major part of the kernel, and if any other terms are used they will be appropriate corrections of insignificant value except when T_H is small. The corrections, if any, should be in exponential form to take advantage of the recursion formula given by (19).

For K_F, no finite number of terms in (8) will adequately represent the kernel as $T_H\to 0+$. For convenience, equation (8) is approximated by using the first term of (6) in its exact form and altering the coefficient of the second term so that

$$K_F \doteq A\frac{\pi}{2}\left[e^{-\pi^2 T_H/4}-e^{-9\pi^2 T_H/4}\right] \tag{22}$$

where A is a normalizing factor given by the ratio of the integrals (6) and (8) as

$$A=\frac{\frac{\pi}{2}\int_0^\infty \sum_{n=0}^{\infty}(2n+1)\exp\left\{-\left[\left(n+\frac{1}{2}\right)\pi\right]^2 T_H\right\}dT_H}{\frac{\pi}{2}\int_0^\infty\left[\exp\left(-\frac{\pi^2}{4}T_H\right)-\exp\left(-\frac{9\pi^2}{4}T_H\right)\right]dT_H}=\frac{1/2}{\frac{2}{\pi}\left(\frac{8}{9}\right)}=0.8835.$$

Although (22) does not accurately represent the kernel K_F for small T_H, it does have the property of starting off with zero value, reaching a peak value, and then decreasing monotonically and exponentially to zero as $T_H\to\infty$, all in conformity with the character of the exact kernel.

For K_Q also, no finite sum of terms given by equation (8) will adequately represent the kernel as $T_H\to 0+$. The character of the curve, however, can be represented by taking only the first term of the series (6) with altered coefficients in the form

$$K_Q \simeq Be^{-\pi^2 T_H/4} \tag{23}$$

where

$$B=\frac{\int_0^\infty \sum_{n=0}^{\infty}\exp\left\{-\left[\left(n+\frac{1}{2}\right)\pi\right]^2 T_H\right\}dT_H}{\int_0^\infty \exp\left(-\frac{\pi^2}{4}T_H\right)dT_H}=\frac{1/2}{4/\pi^2}=1.2337.$$

The approximation for K_Q given by (23) is finite as $T_H\to 0+$, whereas $K_Q\to\infty$ in equation (6). However, the integrals of these kernels enter the computations and converge whether using the exact or approximate kernel.

Although the approximations for the kernels do not accurately agree with the exact kernels, the integrals with respect to time for large t or small H do agree. In any case, the approximations have the characteristics of time history in the convolution integrals and should shed some light on bottom stress time-history.

5. COASTAL BOUNDARY CONDITIONS

In formulating boundary conditions, the artifice of a vertical wall placed at the coast is used. This is done applying the argument that the bottom slope at and near a coast is two or three orders of magnitude greater than the average slope of the Continental Shelf.

In Ekman's equations, for basins with small sloping bottoms, horizontal viscosity at neighboring points is considered small compared to vertical viscosity. This condition no longer holds at coastlines having large bottom slopes and /or the infinite slope of a vertical wall. Thus, to satisfy boundary conditions of a vertical wall placed in the fluid, we would have to consider at least the effects of vertical motion to balance the horizontal viscosity. If Ekman's equation is to be used with coastlines, then compromises are in order.

A physical boundary condition at a coast with a vertical wall has vanishing normal velocities, that is, $u(x,y,z,t)_{x=0}=0$. For transport equations of motion, we settle instead for a more relaxed boundary condition represented by vanishing normal transport, that is, $U(x,y,t)_{x=0}=0$. This relaxed condition permits a useful interpretation of Ekman's equations at the coast. It is possible to postulate a balance between wind and drift *transports* normal to a vertical plane, and this plane can then be regarded as a coastline.

The separate Ekman spirals, drift, and slope currents in the vertical differ, and for finite depths there can be

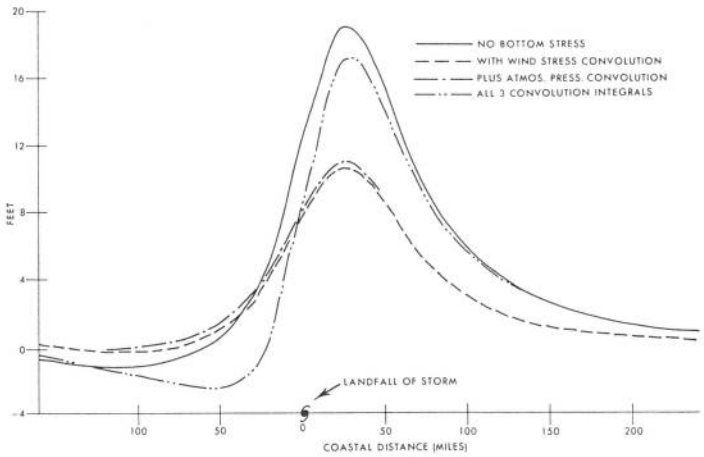

FIGURE 2.—Computed coastal surge profiles at the time of peak surge for various sums of the convolution integrals in the prediction equations. Observer is at sea, facing land; abscissa is the coastline.

at most only a finite number of points in the vertical where the total current has vanishing components in a given horizontal direction. This means that, if bottom stress is considered in Ekman's equation, it is impossible to have both vanishing transport and bottom stress normal to the boundary. We insist, therefore, on vanishing normal transports, $\partial U(x,y,t)/\partial t|_{x=0}=0$, at the coastline and accept the resulting bottom stress values computed by the convolution integrals in (5b) to form

$$-gH\frac{\partial h}{\partial x}+fV+{}^{(x)}F+gH\frac{\partial h_0}{\partial x}-\sum_{j=1}^{3}\mathcal{C}_{(\tau j)}=0. \qquad (24)$$

The above equation is also obtained from equations (41) and (54), the exact analytical expressions for transport, by setting $\mathrm{Re}(\partial/\partial t)(W_{drift}+W_{slope})=0$; in the computations, this is a more convenient form than the boundary condition, $\mathrm{Re}(W_{drift}+W_{slope})=0$.

The boundary equation gives surge gradient and not surge heights; thus, it cannot be used directly to compute coastal surge profiles. The surges on the boundary are determined from the boundary equation by finite-difference techniques using heights at interior points to follow the slope gradient at the boundary.

In the case of no bottom stress, the *dynamic surface slope gradient force balances the driving forces of the storm and the Coriolis force at the boundary.* It may at first appear implausible to balance surface and body forces, but the body forces have been integrated in the vertical so that equation (24) is dimensionally correct. For no bottom stress, the eddy viscosity coefficient does not enter into computations since it is contained implicity in the surface stress and transport terms. This means that ν can take on any value except 0 or ∞. The wind or surface stress by definition does not change, and the transport field always remains the same even though the vertical current profile varies with the fixed parameter ν.

For an example of the results using the boundary equation with bottom stress, consider a storm traveling across a basin from sea to land and normal to a straight-line coast. The nature of the storm, basin, and computational scheme are given in later sections. Figure 2 illustrates coastal surge profiles at the time of peak surge for various elements of the convoluted integral sum in the equations of motion and the boundary equation. Notice the strong effect of the dynamic surface slope on the coastal surge profile.

The boundary depths have not been defined with any precision, since empirical computations demonstrate (for the model storms, basins, and numerical scheme of this study) that the surge profile at the coast is relatively insensitive to any alteration of the coastal depths providing the depths at interior points of the basin are unaltered; this holds even if the boundary depths become small but finite.

To investigate the case of zero boundary depths with bottom stress, one must reformulate the boundary equation. To show this, return to the transport equation of motion (5b) and consider the following functions present in the convolution integrals:

$$\lim_{H\to 0}\frac{2\nu}{H^2}K_F(\tau);\quad \lim_{H\to 0}\frac{2\nu}{H^2}K_Q(\tau).$$

These limits are zero everywhere on the positive T_H axis, except $T_H=0$; the integrals of each function from 0 to ∞ is 1, so that the behavior has the form of a Dirac function. Hence equation (5a) becomes

$$\lim_{H\to 0}\left(\frac{\partial W}{\partial t}=-ifW\right). \qquad (25)$$

(The same result follows if $\nu\to\infty$.) The solution to equation (25) depends on initial values of W, which are zero (or the transports become zero by definition for zero depths); hence, the transport is zero for all times. Now (24) is the same as $\mathrm{Re}(\partial W/\partial t)=0$; so for $H\to 0$, the boundary equation reduces *identically* to zero.

To determine a coastal boundary condition for coastal $H\to 0$, we consider the structure of the vertical current profile for small depths. The exact form for the drift current (after division by H) is given by equation (40) as

$$\frac{u}{H}\Big|_{drift}=\frac{2}{H^2}\sum_{n=0}^{\infty}\cos(2n+1)\frac{\pi}{2}z\int_0^t[{}^{(x)}F(t-\tau)\times\cos f\tau+{}^{(y)}F(t-\tau)\sin f\tau]\times\exp\left\{-\left[(2n+1)\frac{\pi}{2}\right]^2\frac{\nu}{H^2}\tau\right\}d\tau.$$

As $H\to 0$, the limiting form behaves like a Dirac function so that

$$\lim_{H\to 0}\left|\frac{u}{H}\right|_{drift}=\frac{1}{\nu}(1+z)^{(x)}F(t) \qquad (26)$$

since

$$\frac{2}{H^2}\sum_{n=0}^{\infty}\cos(2n+1)\frac{\pi}{2}z\int_0^{\infty}\exp\left\{-\left[(2n+1)\frac{\pi}{2}\right]^2\frac{\nu}{H^2}t\right\}dt$$

$$=\frac{8}{\nu\pi^2}\sum_{n=0}^{\infty}\frac{\cos(2n+1)\frac{\pi}{2}z}{(2n+1)^2}=\frac{1}{\nu}(1+z).$$

(See Dwight 1961.) Interpreting equation (26) for shallow water, we see that the current varies *linearly* with depth and the stress as ${}^{(x)}F(t)$; also, the Coriolis parameter is no longer significant.

From equation (53), the exact form for the slope vertical current profile (after division by H) is given as

$$\left.\frac{u}{H}\right|_{slope}=\frac{2}{H^2}\sum_{n=0}^{\infty}\frac{(-1)^n}{(2n+1)\pi/2}\cos(2n+1)\frac{\pi}{2}z$$
$$\times\int_0^t[{}^{(x)}Q(t-\tau)\cos f\tau+{}^{(y)}Q(t-\tau)\sin f\tau]$$
$$\times\exp\left\{-\left[(2n+1)\frac{\pi}{2}\right]^2\frac{\nu}{H^2}\tau\right\}d\tau.$$

As $H\to 0$, the limiting form also behaves like a Dirac function, so that

$$\lim_{H\to 0}\left.\frac{u}{H}\right|_{slope}=\frac{1}{2\nu}(1-z^2){}^{(x)}Q(t) \tag{27}$$

since

$$\frac{2}{H^2}\sum_{n=0}^{\infty}\frac{(-1)^n}{(2n+1)\pi/2}\cos(2n+1)\frac{\pi}{2}z$$
$$\times\int_0^{\infty}\exp\left\{-\left[(2n+1)\frac{\pi}{2}\right]^2\frac{\nu}{H^2}t\right\}dt$$
$$=\frac{16}{\nu\pi^3}\sum_{n=0}^{\infty}\frac{(-1)^n}{(2n+1)^3}\cos(2n+1)\frac{\pi}{2}z=\frac{1}{2\nu}(1-z^2).$$

(See Dwight 1961.) Interpreting (27) for shallow water, we see that the current varies *parabolically* with depth; the stress is zero on the surface and varies as ${}^{(x)}Q(t)$ on the bottom; the Coriolis parameter is no longer significant.

For vanishing transports normal to a coast, we then form

$$\lim_{H\to 0}\frac{1}{H}\int_{-1}^{0}(u_{drift}+u_{slope})=\frac{1}{\nu}\left[\frac{{}^{(x)}F(t)}{2}+\frac{{}^{(x)}Q(t)}{3}\right]=0$$

or

$${}^{(x)}Q(t)=-\frac{3}{2}{}^{(x)}F(t). \tag{28}$$

Ekman derived the above result for the equilibrium case (Neumann and Pierson 1966). A useful interpretation of the last equation could be as follows. If the characteristic time T_H is 1, then $t_0=H^2/\nu$ is a measure of time to reach equilibrium state. But shallow depths imply $t_0\to 0$, which means that, even near zero, time is large relative to the time required for the equilibrium state to occur. It is emphasized that the 3/2 factor for the coastal boundary condition in (28) occurs only in conjunction with the no-slip bottom boundary condition $w_{z=-1}=0$. For no bottom stress, that is pure bottom slip and $H\to 0$, it follows that ${}^{(x)}Q=-{}^{(x)}F$ as given by equation (24), and the factor is 1.

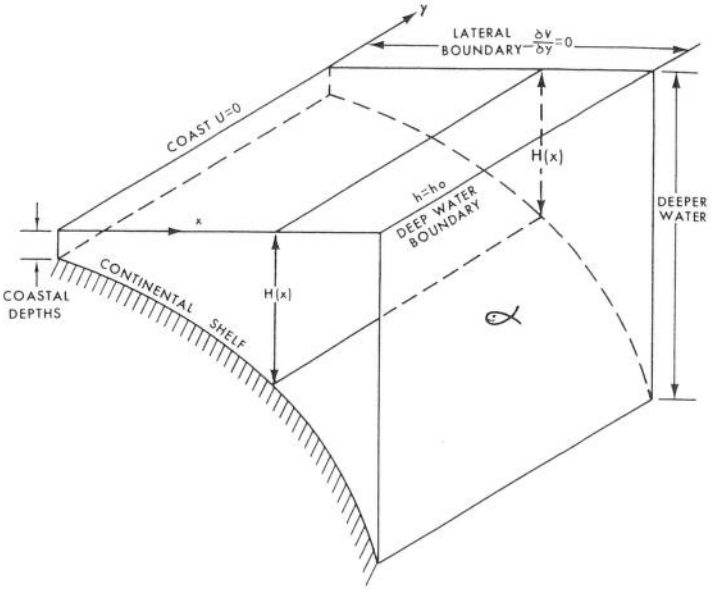

FIGURE 3.—Rectangular one-dimensional variable depth model basin.

The form of the surge in the neighborhood of the seaward boundary is strongly influenced by the depth profile. Suppose at the boundary $H=\alpha x^{\beta}$; α and β are constants. Then taking ${}^{(x)}Q=H\partial h/\partial x$, it is seen that the surge h at the boundary would be finite or infinite as β is less or greater than 1.[6] In particular if $\beta=1$, there is a logarithmic singularity in h.

Nonlinear effects, no doubt, take precedence as $H\to 0$. These effects are not within the scope of this study. Because of this, and since singularities are introduced in the equations of motion, the case of zero boundary depths is not considered in the computational methods of this study.

When the coastal depths are finite, it is possible to determine Q in terms of F as a boundary condition (appendix C). This form of the boundary condition may be preferable to equation (24), for example for Welander's suggested numerical scheme; both forms are identical to within an initial constant, and the initial constant is zero for an initially quiescent sea.

6. MODEL BASINS AND STORMS, OPEN BOUNDARIES, INITIAL CONDITIONS

The model basins of this study correspond to that given by Jelesnianski (1966) consisting of a rectangular-shaped variable depth basin, open to the sea on three sides. Only one-dimensional depth profiles are used since the continental shelves of the oceans vary predominantly in one direction. Except for reprogramming, the need for extra machine core storage, and extra machine time, there are no essential or insurmountable difficulties in the model preventing two-dimensional bottom specifications if such detail is desired. Figure 3 illustrates the idealized basin used in this study.

[6] Natural coastlines generally have $\beta<1$.

For any grid scheme in numerical computations, the grid distance must be fine enough to portray not only the storm surge but also the driving forces of the storm. This distance may be determined by empirical tests. Due to computer core limitations and economics of machine operations, it is impossible at this time to consider an entire ocean as a basin; open boundaries are therefore used in this study.

On the two lateral, open boundaries normal to the coast, the boundary condition used is $\partial V/\partial y=0$. This condition [7] is arbitrary and used purely for convenience. In any case, reflections from these boundaries eventually corrupt the interior of the basin. However, if the boundaries are placed sufficiently far from an area of interest along the coast, there will be a time interval before it is corrupted by reflections from the boundaries. The placement of these side boundaries are determined by empirical tests.

The deep water open boundary is placed somewhat arbitrarily near the juncture of the continental shelf and slope. In deep water away from coastal influences, the dynamic surge is small, and the surface heights correspond very closely to the inverse barometric effect. The boundary condition used is $h=h_0$.

The model storms used in this study are analytically described using simple meteorological parameters presumably available at weather stations. For the formulation of the model storm, see Jelesnianski (1966).

The fluid in the basin is initially quiescent. The storm is allowed to grow to maturity in a continuous but rapid manner. Initial positioning of the storm is unimportant if the placement of the *mature* storm lies in deep water beyond the Continental Shelf. For storms traveling more or less parallel to the coast and along the Continental Shelf, initial placement must be at least sufficiently distant from the area of interest so that the surge has time to form; this can be operationally determined by empirical tests through variation of initial storm placement, growth time of storm, basin length, etc.

7. TESTING THE MODEL

Prior to testing the model with actual observations, a value for the eddy viscosity coefficient ν is required. To see how the coastal surge profile varies for different values of ν, consider a particular model storm traveling normal to the coast of a model basin. Figure 4 is a plot of computed surge profiles at the time of peak surge. For small ν, the profile [8] approaches the no bottom stress profile. By comparing the observed surges from tide gages against computed surges of the model, it is possible to choose a value of ν to adequately match the observed surges.

The most complicated coastal surge phenomena occur for storms moving more or less parallel to the coast. It was decided, therefore, to test the model for such storms by comparing it with observed storm surges off Atlantic City. Only on the Atlantic Seaboard do historical storms have tracks nearly parallel to a coast, and Atlantic City is the only station in this region that has a tide gage well exposed to the sea.

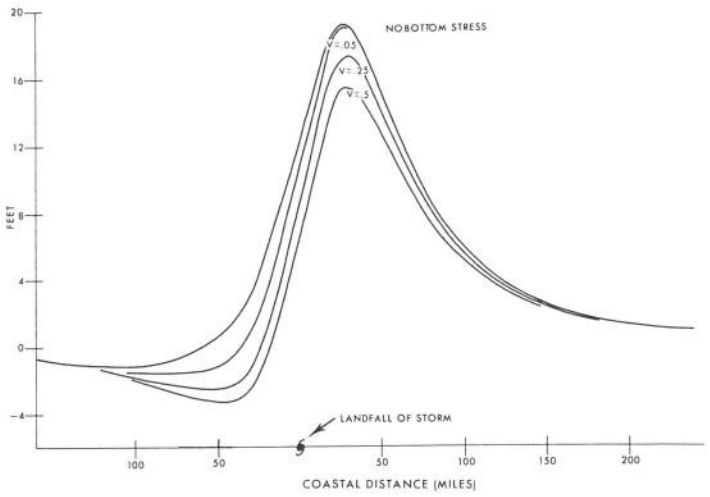

FIGURE 4.—Coastal storm surge profiles for different eddy viscosity values. All other variables are the same; abscissa is the coastline.

Figure 5 shows the paths of three storms on which computations made in this study were based. The plan view of the model basin is 560×65 mi. The depths of the model basin vary in one dimension only and are equivalent to the mean depths in the region off Atlantic City. Initially, the storms were placed at the + points in the figure, with zero strength. While traveling along their tracks, they were allowed to grow to maturity in a rapid but continuous manner over 2 hr. The observed meteorological storms varied in strength, size, and speed of motion along their tracks. The meteorological parameters used to describe the model storms were supplied by the Hydrometeorological Branch, Water Management Information Division, Office of Hydrology, ESSA, Silver Spring, Md.; they are not listed in this study. For computational convenience, the fixed storm parameters in the model were altered only once every hour to correspond with the observed or extrapolated synoptic data of the storms.

Figure 6 shows an observed tide record for the Atlantic City tide gage during passage of the September 1944 storm. It was necessary to put the raw observed tide data in suitable form before effecting comparisons between observed and computed data. The sequential numbers on the tide record represent hourly times of tide heights reported by the Coast and Geodetic Survey. The hourly records do not adequately portray the low-frequency oscillations; data between the hourly records were therefore supplied by smoothing the high-frequency oscillations of the tide record by eye. The astronomical and seasonal tides were then subtracted from the prepared tide record using methods described by Harris (1963). This type of processed data will henceforth be referred to as observed data.

Figure 7 compares computed versus observed tides at Atlantic City for the 1944 storm whose path is illustrated

[7] One could postulate radiation properties, such as making the two boundaries transparent to waves, say traveling parallel to the coast. For example, it is possible to form traveling waves with phase speed equal to the speed of the storm traveling parallel to the coast (Jelesnianski 1966).

[8] The profiles computed by Platzman's method (Jelesnianski 1967) behave somewhat similarly except for the important difference that the peak surge for small ν exceeds the peak surge of the no bottom stress case.

in figure 6. The peak tide, computed with and without bottom stress, agrees very well with the observed peak and time of occurrence. This is to be expected, since the peak is directly associated with the storm center and for *fast moving storms* the characteristic Ekman time $t=H^2/\nu$ is too large for bottom stress to be significantly felt under the storm center. After passage of the storm center and with the passing of time, the resulting waveforms or resurgences in the basin are then affected by bottom stress as demonstrated by the figure. The resurgences computed with and without bottom stress have almost equal amplitude and phase until contaminated by reflections from the false open-boundaries. With bottom stress, the resurgences decrease in amplitude with time, but with very little phase change [9] as compared to no bottom stress. Figures 8 and 9 show computed results for the two remaining storms. In all these computations, ν was given the value 0.15 ft^2/sec (139 cm^2/sec).

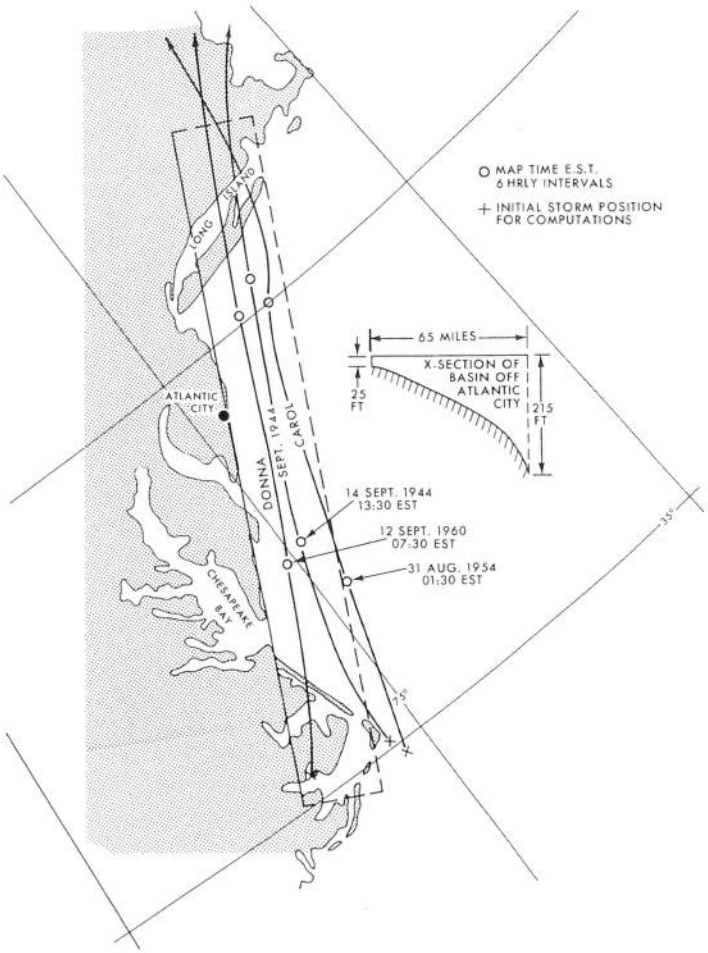

FIGURE 5.—Observed paths of three storms along the Atlantic Seaboard. The model basin position is shown by a rectangle.

On the eastern seaboard, there are insufficient tide gages to determine the character of the observed coastal surge profile. Figure 10 illustrates the time history of the computed surge profile on the coast for the September 1944 storm. The directly generated crest and trough associated with the storm center, and moving with it, decrease in amplitude with time due to decreasing storm strength. The nature of the following resurgences are not discussed except to point out that phase speeds are not equal to storm speed.

Traveling waves, with phase speed equal to storm speed, can form for the storm sizes in the model of this study, but they depend in part on the nearshore bottom topography. To demonstrate this, consider the model basin off Atlantic City modified now to a shallow linear depth as shown in the insert of figure 11; when the September 1944 storm surge is recomputed in this modified basin, the resurgences (fig. 11) appear to be traveling waves with phase speed equal to storm speed.

The resurgences computed with bottom stress in this study agree in essence with the observed resurgences, but there are unexplained phenomena. For example, in figure 8 (hurricane Donna), there is an observed spike at 1400 EST that was not reproduced in the computations; a similar but less pronounced spike exists in figure 7.

The driving forces of a storm can excite certain wave forms that become trapped in a basin (Longuet-Higgins

[9] In Platzman's method (Jelesnianski 1967), there are significant phase changes.

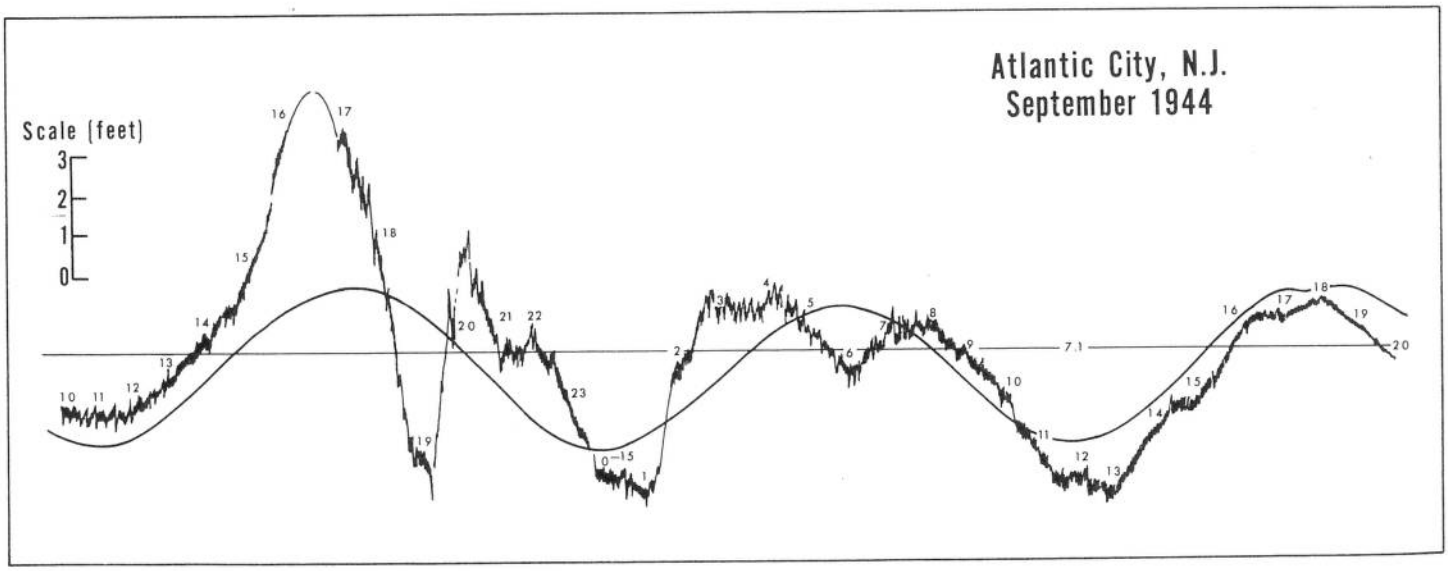

FIGURE 6.—Recorded tide traced from original gage record, and predicted astronomical tide (smooth curve) at Coast and Geodetic Survey Tide Station, Steel Pier, Atlantic City, N.J. The integers are hourly reported tide heights (reproduced by permission of Harris 1963).

FIGURE 7.—Comparing the observed and computed surges at Atlantic City for the September 1944 storm (zero time at initialization for computations).

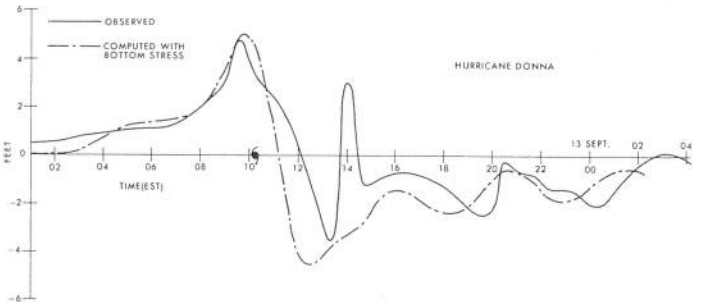

FIGURE 8.—Observed and computed surges at Atlantic City for hurricane Donna.

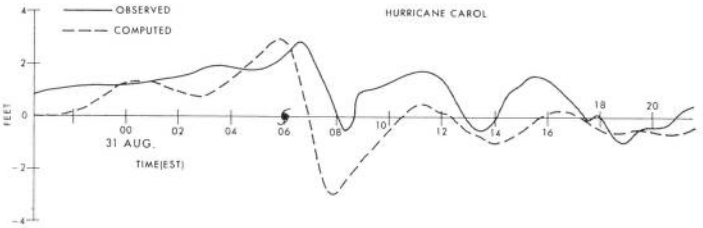

FIGURE 9.—Observed and computed surges at Atlantic City for hurricane Carol.

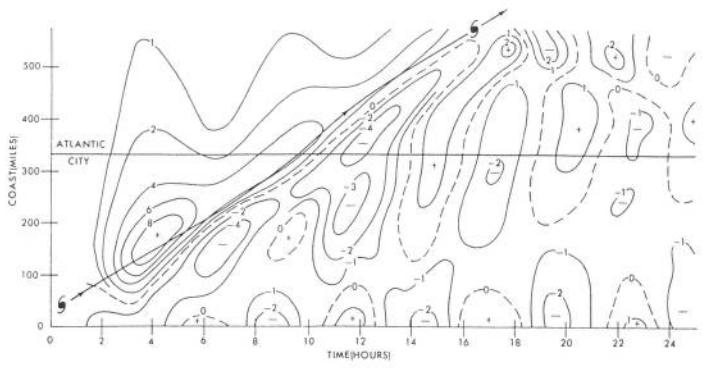

FIGURE 10.—Time history of the computed coastal surge profile for the September 1944 storm. Arrows show the path of the storm relative to the coast (storm initially 40 mi from bottom boundary).

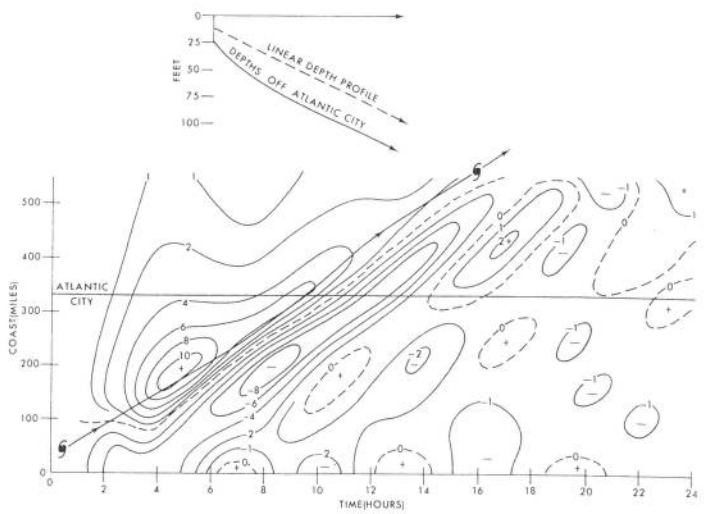

FIGURE 11.—Same as figure 10, but using the shallow, linear depth basin shown by the broken line depth profile in the insert.

1967), and these trapped waves produce resurgences. The phenomena of trapped waves is beyond the scope of this study. It is suggested that the application of geometric optics, or ray theory, could be a fruitful venture to shed light on possible trapped waves for any given basin (Shen and Meyer 1967).

Many simplifying assumptions are used in the model. No account is taken of the interaction between transient surges, the basic flow of the general oceanic circulation, and the astronomical tides. Curvilinear boundary coasts, estuaries, and two-dimensional depth profiles have been ignored. Notwithstanding the simplified treatment, there is reasonable agreement between observed and computed surges.

8. SUMMARY AND CONCLUSIONS

A model storm described analytically with simple meteorological parameters is used to represent observed tropical storms and thereby to compute driving forces that generate storm surges. These surges are computed by numerical means in a rectangular-shaped model basin with depths varying in one dimension, and open to the sea on three sides.

To test the model used in this study, computed surges for three storms traveling parallel to the eastern seaboard of the United States are compared with observed surges at Atlantic City. Ekman's equation of motion in transport form was found to be very useful when bottom stress was put in a convoluted form to take into account its time history at local points of the basin. The exact form of the integral is cumbersome to work with, but a simple representation of the kernel in the convolution integral gave a recursive relation in convenient form for numerical computations.

The computed results do not differ greatly from those of a differential form for bottom stress given by Platzman (1963) and computed by Jelesnianski (1967), except that ...tegral form was better behaved for small values of the eddy viscosity and there were smaller phase changes in the post storm resurgences following passage of the

model storm. The integral form is not truncated as is the differential form, and it retains all the time-history bottom stress generated by driving forces; this serves to eliminate awkward questions on convergence properties of bottom stress formulation. For more realistic modeling of bottom stress, extra machine computations are required for the preliminary application of this study.

A time-dependent coastal boundary condition was developed by balancing drift and slope transports normal to a vertical wall. This boundary condition was then specialized in a form containing bottom stress and convenient for computations; it cannot, however, handle zero boundary depths. A separate time-dependent boundary condition that agrees with Ekman's classical equilibrium case was formed for zero depths. A defect at the coastal boundary is that Ekman's equation uses vanishing transport that in turn does not imply vanishing current. Thus, the boundary condition is only a first approximation that is hopefully acceptable for the present state of the art in storm surge computations.

The results of this study explain many of the observed phenomena of storm surges, but there are some unexplained anomalies. These anomalies may in part be due to unknown or unobserved meteorological activity in the storms, the gross simplicity of the model basin, and initialization or starting procedures in the basin. Of equal significance may be the coarseness of the grid spacing, which cannot recognize small-scale resonance phenomena restricted to a small region about the coast. Even within the linear equation limitations of this study, further research is required to include the effects from curvilinear coastlines, two-dimensional variable depth basins, the effects of open boundary conditions on interior points of the basin, and the errors introduced by nonvanishing currents normal to a coast with finite depths. Further insight may also be gained by considering a bottom slip condition rather than vanishing bottom current.

APPENDIX A

A bottom stress formulation, necessary in equation (2), can be determined rather easily by means of a table of Laplace transforms, without requiring an explicit solution of the vertical current profile. However, the transport vertical current profile is directly formulated to analytically investigate special problems such as transport formation in deep and shallow waters, the formation of coastal currents, the transient surface slope, and comparisons with Ekman's equilibrium cases.

The vertical current profile is composed of drift and slope currents. In this section, separate solutions in convoluted form are given for these currents in terms of surface slope and surface wind stress. A superposition of the solutions gives the general vertical current profile. The vertical gradient of this current on the bottom then gives a form for the bottom stress. Coastal boundaries are not considered since special techniques, given in the main report, are used to handle these boundaries. It is convenient to form the solutions in terms of a nondimensional characteristic time parameter, $T_H=(\nu/H^2)t$.

VERTICAL CURRENT PROFILES AND BOTTOM STRESS SOLUTIONS FOR LARGE T_H

Pure drift current—Ekman's equation for pure drift current is, with the notation of equation (2),

$$\frac{\partial w}{\partial t}=-ifw+\frac{\nu}{H^2}\frac{\partial^2 w}{\partial z^2} \tag{29}$$

with boundary conditions

$$w(-1,\,t)=0,\ \frac{\nu}{H}\frac{\partial w}{\partial z}\bigg|_{z=0}=F(t);\ \frac{\partial^n w}{\partial t^n}\bigg|_{t=0}=0,\ n=0,\,1.$$

The Laplace transform of (29) is

$$s\hat{w}(z,s)=-if\hat{w}(z,s)+\frac{\nu}{H^2}\frac{\partial^2\hat{w}(z,s)}{\partial z^2} \tag{30}$$

with remaining boundary conditions

$$\hat{w}(-1,s)=0,\ \frac{\nu}{H}\frac{\partial\hat{w}(z,s)}{\partial z}\bigg|_{z=0}=\hat{F}(s).$$

For preliminary considerations, and comparisons with classical solutions, let the surface stress be a suddenly applied constant force iF_0 and let the resulting current for this special case be w_0. The solution to equation (30) is

$$\hat{w}_0=\frac{iHF_0}{\nu s\alpha}\frac{\sinh\alpha(1+z)}{\cosh\alpha};\ \alpha=\sqrt{\frac{if+s}{\nu/H^2}}. \tag{31}$$

A solution for the above, using an inversion integral, is

$$w_0(z,\,t)=\frac{1}{2\pi i}\int_{a-ib}^{a+ib}e^{st}\hat{w}_0(z,s)ds=\Sigma\text{ residues}. \tag{32}$$

The poles of (31) are all simple. The residues from these poles are given in table 1 where $n=0,1,2,\ldots$, $\gamma=(1+i)\,EH$, $E=\sqrt{f/2\nu}$ (Ekman's parameter), and $\beta_n=[n+(1/2)]\pi/H$.

A solution for equation (31) is then

$$w_0(z,\,t)=\frac{iHF_0}{\nu\alpha}\frac{\sinh[\gamma(1+z)]}{\cosh\gamma}-\frac{iF_0}{\nu H}\sum_{n=0}^{\infty}A_n\cos\left[\left(n+\frac{1}{2}\right)\pi z\right]e^{-\theta_n t} \tag{33}$$

where

$$A_n=\frac{2\beta_n^2-4iE^2}{\beta_n^4+4E^4};\ \theta_n=\nu[2iE^2+\beta_n^2]=if+\nu\beta_n^2.$$

Equation (33) may also be written as

$$w_0(z,\,t)=\frac{iF_0}{\nu H}\sum_{n=0}^{\infty}A_n\cos\left[\left(n+\frac{1}{2}\right)\pi z\right]\{1-e^{-\theta_n t}\} \tag{34}$$

since

$$\frac{H}{\nu\gamma}\frac{\sinh[\gamma(1+z)]}{\cosh\gamma}=\frac{1}{\nu H}\sum_{n=0}^{\infty}A_n\cos\left[\left(n+\frac{1}{2}\right)\pi z\right]$$

on setting $t=0$ in equation (33).

Equation (33) is identical to the solution given by Nomitsu (1933*a*) using other methods; Nomitsu plotted hodographs for different depth basins with Ekman's number as a parameter. Similar solutions have been obtained by Fjeldstad (1929) and Hidaka (1933) using integral equations.

TABLE 1.—*Residues of the poles of equation (31)*

Poles	Residues
$s=0$	$\frac{iHF_0}{\nu\gamma}\frac{\sinh[\gamma(1+z)]}{\sinh\gamma}$
$s=-if$	0
$s_n=-\left[if+\frac{\nu}{H^2}\left(n+\frac{1}{2}\right)^2\pi^2\right]$	$-\frac{iF_0[2\beta_n^2-4iE^2]}{\nu H[4E^4+\beta_n^4]}\cos\left[\left(n+\frac{1}{2}\right)\pi z\right]e^{-\nu(2iE^2+\beta_n^2)t}$

Before proceeding to more general cases of variable surface stress, it is interesting to compare the equilibrium transport of equation (34) with Ekman's classical solution for the case of infinite depths. To do this, (34) is integrated in the vertical to form

$$\frac{1}{H}W_0(t)=\frac{iF_0}{\nu H}\sum_{n=0}^{\infty}\frac{(-1)^nA_n}{H\beta_n}\{1-e^{-\theta_n t}\}. \tag{35}$$

In the above, the operations of summation and integration were interchanged; this is permissible since the series (34) is uniformly and absolutely convergent in the range of integration. Equation (35) can be now written as

$$W_0=\frac{iF_0}{\nu}\sum_{n=0}^{\infty}\frac{(-1)^n2\left[\left(n+\frac{1}{2}\right)\frac{\pi}{H}\right]^2-4iE^2}{\left[\left(n+\frac{1}{2}\right)\frac{\pi}{H}\right]^4+4E^4}\frac{1}{\pi\left(n+\frac{1}{2}\right)}$$
$$\times\left\{1-\exp[-ift]\exp\left\{-\left[\left(n+\frac{1}{2}\right)\pi\right]^2\frac{\nu t}{H^2}\right\}\right\}. \tag{36}$$

At this point, there is a choice in limit procedures. Consider

$$\lim_{\substack{t\to\infty\\H\to\infty}}W_0=\frac{iF_0}{\nu}\sum_{n=0}^{\infty}\frac{-(-1)^n4iE^2}{4E^4}\frac{1}{\pi\left(n+\frac{1}{2}\right)}=\frac{F_0}{f}$$

and

$$\lim_{\substack{H\to\infty\\t\to\infty}}W_0=\frac{iF_0}{\nu}\sum_{n=0}^{\infty}\frac{-(-1)^n4iE^2}{4E^4}\frac{1}{\pi\left(n+\frac{1}{2}\right)}[1-e^{-ift}]$$
$$=\frac{F_0}{f}[1-e^{-ift}]. \tag{37}$$

The first limiting case is Ekman's classical solution for transport in an infinite depth basin. The second limiting case demonstrates that, in limiting procedures, care must be exercised on how the question of limits is asked. A simple physical interpretation could be as follows. Ekman assumes that a balance between input momentum and dissipation exists without specifying how the balance was reached. In the latter equation of (37), the depths are too large for bottom stress to act as a dissipating mechanism; hence, the only way remaining to balance momentum is for the fluid to work against the surface stress cyclically with time. This suggests that, for deep water systems, an internal dissipating mechanism should be considered. A very simple one could be the Guldberg-Mohn assumption where internal friction is given by $-rw$, r a constant. Equation (29) could then be written as

$$\frac{\partial w}{\partial t}=-if'w+\frac{\nu}{H^2}\frac{\partial^2 w}{\partial z^2};\ f'=f-ir. \tag{38}$$

Replacing f with f' in (36), one finds that the sequence H, $t\to\infty$, or t, $H\to\infty$ is now irrelevant. The transport, of course, is now no longer 90° cum sole to the wind stress, but skewed by the angle $\tan^{-1}r/f$. Since $f\gg r$, except at or very near the Equator, internal viscosity is not very important in transient solutions except at small latitudes or large depths. In this study, only the shallow continental shelf is used so that for practical considerations internal viscosity effects are small compared to bottom stress during transient conditions.

It is desirable to remove the restriction of a constant wind stress. Suppose the wind stress varies with time, but with the initial property of $F(0)=0$ and $\partial F/\partial t|_{t=0}=0$. Then the solution to equation (30) is

$$\hat{w}(z,s)=s\hat{F}(s)\hat{w}_0(z,s). \tag{39}$$

The solution to the above can immediately be written as

$$w(z,t)=-\int_0^t\frac{\partial F(t-\tau)}{\partial\tau}w_0(z,\tau)d\tau.$$

Inserting equation (34) into the above, integrating by parts, and noting that $A_n\theta_n=2\nu$, one finds the drift current to be

$$w(z,t)=\frac{2}{H}\sum_{n=0}^{\infty}\cos\left[\left(n+\frac{1}{2}\right)\pi z\right]\int_0^t F(t-\tau)e^{-\theta_n\tau}d\tau. \tag{40}$$

The drift transport is

$$W=2\sum_{n=0}^{\infty}\frac{(-1)^n}{H\beta_n}\int_0^t F(t-\tau)e^{-\theta_n\tau}d\tau. \tag{41}$$

From equation (40), the drift current bottom stress becomes

$$\frac{\nu}{H}\frac{\partial w}{\partial t}\bigg|_{z=-1}=\frac{2\nu}{H}\int_0^t F(t-\tau)\sum_{n=0}^{\infty}(-1)^n\beta_n e^{-\theta_n\tau}d\tau$$

or

$$\frac{\nu}{H}\frac{\partial w}{\partial z}\bigg|_{z=-1}=\frac{2\nu}{H^2}\int_0^t F(t-\tau)e^{-ift}K_F(\tau)d\tau \tag{42}$$

where

$$K_F(t)=\sum_{n=0}^{\infty}(-1)^n\pi\left(n+\frac{1}{2}\right)\exp\left\{-\left[\left(n+\frac{1}{2}\right)\pi\right]^2\frac{\nu}{H^2}t\right\}.$$

Slope current—Ekman's equation for slope current is, with the notation of equation (2),

$$\frac{\partial w}{\partial t}=-ifw+\frac{\nu}{H^2}\frac{\partial^2 w}{\partial z^2}+q \tag{43}$$

with boundary conditions

$$w(-1,t)=0;\ \frac{\nu}{H}\frac{\partial w}{\partial z}\bigg|_{z=0}=0;\ \frac{\partial^n w}{\partial t^n}\bigg|_{t=0}=0,\ n=0,1.$$

Let the surface slope q_0 be constant and the current for this special case w_0. When using Laplace procedures as

in drift current,

$$\hat{w}_0(z,s)=\frac{H^2q_0}{\nu s\alpha^2}\left[1-\frac{\cosh\alpha z}{\cosh\alpha}\right] \text{ and } \alpha=\sqrt{\frac{if+s}{\nu/H^2}}. \quad (44)$$

The inversion integral of the above, with identical poles as in drift current, gives a solution of

$$w_0(z,t)=\frac{q_0}{if}\left[1-\frac{\cosh\gamma z}{\cosh\gamma}\right] -\frac{q_0}{\nu H}\sum_{n=0}^{\infty}\frac{(-1)^nA_n}{\beta_n}\cos\left[\left(n+\frac{1}{2}\right)\pi z\right]e^{-\theta_n t}. \quad (45)$$

When setting $t=0$ in the above,

$$\frac{1}{if}\left[1-\frac{\cosh\gamma z}{\cosh\gamma}\right]=\frac{1}{\nu H}\sum_{n=0}^{\infty}\frac{(-1)^nA_n}{\beta_n}\cos\left[\left(n+\frac{1}{2}\right)\pi z\right]. \quad (46)$$

Equation (45) can then be written as

$$w_0(z,t)=\frac{q_0}{\nu H}\sum_{n=0}^{\infty}\frac{(-1)^nA_n}{\beta_n}\cos\left[\left(n+\frac{1}{2}\right)\pi z\right]\{1-e^{-\theta_n t}\}. \quad (47)$$

This solution is identical to the one given by Nomitsu (1933*b*) using other methods.

Before proceeding to more general cases of variable surface slope, it is interesting to compare the equilibrium transport of equation (47) with Ekman's classical solution for infinite depths. For one to accomplish this, equation (47) is integrated in the vertical to form

$$W_0(t)=\frac{q_0}{\nu H}\sum_{n=0}^{\infty}\frac{(-1)^nA_n}{\beta_n^2}[1-e^{-\theta_n t}]. \quad (48)$$

If $t\to\infty$, then

$$\lim_{t\to\infty}W_0=\frac{q_0}{\nu H}\sum_{n=0}^{\infty}\frac{(-1)^nA_n}{\beta_n^2}. \quad (49)$$

If (46) is integrated in the vertical, then

$$\frac{1}{\gamma}\tanh\gamma=1-\frac{ifH^2}{\nu}\sum_{n=0}^{\infty}\frac{(-1)^nA_n}{\beta_n^2}.$$

Substituting the above into equation (48) gives

$$\lim_{t\to\infty}W_0=\frac{q_0H}{if}\left[1-\frac{1}{\gamma}\tanh\gamma\right]=\frac{iq_0H}{f} \times\left[-1+\frac{1}{2EH}\frac{\sinh 2EH+\sin 2EH}{\cosh 2EH+\cos 2EH} +\frac{i}{2EH}\cdot\frac{-\sinh 2EH+\sin 2EH}{\cosh 2EH+\cos 2EH}\right] \quad (50)$$

and

$$\lim_{\substack{t\to\infty\\H\to\infty}}U_0=\frac{q_0}{2fE}, \quad (51)$$

that is, Ekman's classical solution for slope transport. If the above limiting procedure had been reversed, then there would be a factor $(1-e^{-ift})$ just as in the pure drift-current case.

Suppose now that the surface slope varies with time and the initial conditions [10] are $q(0)=0$ and $\partial q/\partial t|_{t=0}=0$. Then

$$\hat{w}(z,s)=s\hat{q}(s)\hat{w}_0(z,s). \quad (52)$$

The solution to the above can be immediately written as

$$w(z,t)=-\int_0^t\frac{\partial q(t-\tau)}{\partial\tau}w_0(z,\tau)d\tau.$$

When inserting equation (47) into the above and integrating by parts, the slope becomes

$$w(z,t)=\frac{2}{H}\sum_{n=0}^{\infty}\frac{(-1)^n}{\beta_n}\cos\left[\left(n+\frac{1}{2}\right)\pi z\right]\int_0^t q(t-\tau)e^{-\theta_n\tau}d\tau. \quad (53)$$

The slope transport is

$$W(t)=\frac{2}{H}\sum_{n=0}^{\infty}\frac{1}{\beta_n^2}\int_0^t q(t-\tau)e^{-\theta_n\tau}d\tau. \quad (54)$$

From equation (53), the slope current bottom stress becomes

$$\frac{\nu}{H}\frac{\partial w}{\partial z}\bigg|_{z=-1}=\frac{2\nu}{H}\int_0^t q(t-\tau)\sum_{n=0}^{\infty}e^{-\theta_n\tau}d\tau$$

or

$$\frac{\nu}{H}\frac{\partial w}{\partial z}\bigg|_{z=-1}=\frac{2}{H^2}\int_0^t Q(t-\tau)e^{if\tau}K_Q(\tau)d\tau \quad (55)$$

where

$$K_Q(t)=\sum_{n=0}^{\infty}\exp\left\{-\left[\left(n+\frac{1}{2}\right)\pi\right]^2\frac{\nu}{H^2}t\right\}.$$

BOTTOM STRESS SOLUTIONS FOR SMALL T_H

Pure drift current—Consider equation (31) with a variable wind stress so that

$$\hat{w}(z,s)=\hat{F}(s)\hat{G}(z,s) \quad (56)$$

where

$$\hat{G}(z,s)=\frac{H}{\nu\alpha}\frac{\sinh\alpha(1+z)}{\cosh\alpha},\ \alpha=\frac{s+if}{\nu/H^2}.$$

If a solution for bottom stress *only* is desired, it is not necessary to solve for the vertical current profile. Bottom stress is given as

$$\frac{\nu}{H}\frac{\partial\hat{w}}{\partial z}\bigg|_{z=-1}=\frac{\nu}{H}\hat{F}\frac{\partial\hat{G}}{\partial z}\bigg|_{z=-1}=\hat{F}\operatorname{sech}\alpha. \quad (57)$$

The inversion of sech α, from Laplace transform tables, immediately gives equation (42) for large T_H. To consider small T_H, rearrange sech α as

$$\operatorname{sech}\alpha=\frac{2e^{-\alpha}}{1+e^{-2\alpha}}=2\sum_{n=0}^{\infty}(-1)^ne^{-(2n+1)\alpha}. \quad (58)$$

The following inversions

$$\mathcal{L}^{-1}[e^{-a\sqrt{s}}]=\frac{a}{2\sqrt{\pi t^3}}e^{-a^2/4t} \text{ and } \mathcal{L}^{-1}[\hat{G}(cs-b)]=\frac{1}{c}e^{bt/c}G(t/c),$$

[10] For initial conditions, care must be taken that $q=0$ for $t\le 0$. In appendix C, it is shown that the dynamic slope at a *coastal* boundary for an initially quiescent sea and surface stress $F(t)$ jumps immediately to $q(0)=-F(0)/H$. Thus it is required that $F(t)=0$ for $t\le 0$; if F is a constant, then it is required to consider a step function that changes in value from 0 to F at $t=0$.

from any table of Laplace transforms applied to (58), gives for equation (57)

$$\frac{\nu}{H}\frac{\partial w}{\partial z}\bigg|_{z=-1}=\frac{2\nu}{H^2}\int_0^t F(t-\tau)e^{-if\tau}K_F(\tau)d\tau$$

where

$$K_F(t)=\frac{1}{\sqrt{\pi}\left(\frac{\nu t}{H^2}\right)3/2}\sum_{n=0}^{\infty}(-1)^n\left(n+\frac{1}{2}\right)\times\exp\left[-\left(n+\frac{1}{2}\right)^2\Big/(\nu t/H^2)\right]. \quad (59)$$

The interchange of summation and Laplace inversion is justified, since the series in (58) is absolutely convergent on the lines (Re (s)=constant) on which the inversion integral is defined. The convergence properties of the above kernel are discussed in the main report.

Pure slope current—Consider equation (44) with a variable surface slope so that

$$\hat{w}(z,s)=\hat{Q}(s)\hat{G}(z,s) \quad (60)$$

where

$$\hat{G}(z,s)=\frac{H}{\nu\alpha^2}\left[1-\frac{\cosh\alpha z}{\cosh\alpha}\right]\text{ and }\alpha=\sqrt{\frac{s+if}{\nu/H^2}}.$$

Bottom stress is given as

$$\frac{\nu}{H}\frac{\partial\hat{w}}{\partial z}\bigg|_{z=-1}=\hat{Q}\frac{\tanh\alpha}{\alpha}. \quad (61)$$

The inversion of $\tanh\alpha/\alpha$, from Laplace transform tables, immediately gives the expansion of (55) in terms of large T_H. The expansion in terms of small T_H is obtained by rearranging $\tanh\alpha/\alpha$ as

$$\frac{\tanh\alpha}{\alpha}=\frac{1-e^{-2\alpha}}{\alpha(1+e^{-2\alpha})}=\frac{1}{\alpha}\left[1+2\sum_{n=1}^{\infty}(-1)^n e^{-(2n+1)\alpha}\right]. \quad (62)$$

The following inversions

$$\mathcal{L}^{-1}\left[\frac{1}{\sqrt{s}}\right]=\frac{1}{\sqrt{\pi t}},\ \mathcal{L}^{-1}\left[\frac{e^{-a\sqrt{s}}}{\sqrt{s}}\right]=\frac{e^{-a^2/4t}}{\sqrt{\pi t}},\text{ and }\mathcal{L}^{-1}[\hat{G}(cs-b)]=\frac{1}{c}e^{bt/c}G(t/c),$$

from any table of Laplace transforms applied to (62), gives for equation (61)

$$\frac{\nu}{H}\frac{\partial w}{\partial z}\bigg|_{z=-1}=\frac{2\nu}{H^2}\int_0^t Q(t-\tau)e^{-if\tau}K_Q(\tau)d\tau$$

where

$$K_Q(t)=\frac{1}{2\sqrt{\pi t\nu/H^2}}\left\{1+2\sum_{n=1}^{\infty}(-1)^n\times\exp\left[-\left(n+\frac{1}{2}\right)^2\Big/(t\nu H^2)\right]\right\}. \quad (63)$$

The convergence properties of the above kernel are discussed in the main report.

APPENDIX B

Recourse is made to Lebesgue's dominated convergence theorem for improper integrals (Apostol 1967, Riesz 1955) to justify the exchange of summation and integration operations for the exact kernels in equation (6).

LEBESGUE'S THEOREM

If the functions $f_n(t)$, assumed summable in the interval (a,b), converge almost everywhere to a function $f(t)$ and if furthermore there exists a summable function $g(t)$ such that $|f_n(t)|\leq g(t)$ for all n, then the function $f(t)$ is also summable and

$$\int_a^b f_n(t)dt\to\int_a^b f(t)dt.$$

Using the notation of Apostol (1967), one finds the above to be

$$\lim_{n\to\infty}\int_a^b f_n(t)dt=\int_a^b\lim_{n\to\infty}f_n(t)dt=\int_a^b f(t)dt. \quad (64)$$

Since the exact kernels are uniformly convergent for all ranges of positive t except neighborhoods of $t=0$, then only a small range, say 0 to 1, needs to be retained in the limits of integration. Consider now only the pertinent form of the exact kernel K_F in equation (6)

$$\int_0^1\sum_{n=0}^{N}(-1)^n\frac{\exp\left[-\left(n+\frac{1}{2}\right)^2 t\right]}{\left(n+\frac{1}{2}\right)}dt=\int_0^1 f_n(t)dt.$$

To develop the summable function $g(t)$, consider

$$|f_n(t)|\leq\sum_{n=0}^{N}\left\{\frac{\left(\frac{1}{2}\right)^{2\epsilon}\exp\left[-\left(n+\frac{1}{2}\right)^2 t\right]}{\left(n+\frac{1}{2}\right)^{1-2\epsilon}t^{(1/2)-\epsilon}}t^{(1/2)}\right\}t^{-\epsilon}\leq t^{-\epsilon}\left(\frac{1}{2}\right)^{-2\epsilon}\times\int_0^{\infty}\frac{e^{-r^2}}{r^{1-2\epsilon}}dr$$

where $0<\epsilon<1$. Now let

$$g(t)=t^{-\epsilon}\left(\frac{1}{2}\right)^{-2\epsilon}\int_0^{\infty}\frac{e^{-r^2}}{r^{1-2\epsilon}}dr=2^{2\epsilon-1}t^{-\epsilon}\,\Gamma(\epsilon) \quad (65)$$

where $\Gamma(\epsilon)$ is standard notation for the gamma function that is finite when $\epsilon>0$. But then $|f_n(t)|\leq g(t)$, and $\int_0^1 g(t)dt$ converges; therefore, equation (64) follows. A similar proof holds for the exact K_Q kernel, so the integral and summation operators can be interchanged.

APPENDIX C

For coastal boundary conditions, it may be preferable to determine ${}^{(x)}Q$, the surface gradient, in terms of ${}^{(x)}F$, the surface stress. This relation does not determine the coastal surges; however, they can be computed by extrapolating surge heights on interior points of the basin to agree with ${}^{(x)}Q$ on the boundary. Consider the boundary condition

$$\text{Re}\,(W_{drift}+W_{slope})=0. \quad (66)$$

Note that the above differs from the boundary condition (24) where $\mathrm{Re}(\partial/\partial t)\ (W_{drift}+W_{slope})=0$.

To start, one writes equation (66) in terms of the approximate kernels given by (22) and (23); later, the exact kernels will be considered. From equations (41) and (54),

$$W_{drift}+W_{slope}=2\sum_{n=0}^{\infty}\frac{(-1)^n}{\left[(2n+1)\frac{\pi}{2}\right]}\times\int_0^t F(t-\tau)\exp(-if\tau)\exp\left\{-\left[(2n+1)\frac{\pi}{2}\right]^2\frac{\nu\tau}{H^2}\right\}d\tau+2\sum_{n=0}^{\infty}\frac{1}{\left[(2n+1)\frac{\pi}{2}\right]^2}\int_0^t Q(t-\tau)\exp(-if\tau)\times\exp\left\{-\left[(2n+1)\frac{\pi}{2}\right]^2\frac{\nu\tau}{H^2}\right\}d\tau. \quad (67)$$

From equations (22) and (23),

$$K_F(t)=\sum_{n=0}^{\infty}(-1)^n(2n+1)\frac{\pi}{2}\exp\left\{-\left[(2n+1)\frac{\pi}{2}\right]^2\frac{\nu}{H^2}t\right\}\doteq A\frac{\pi}{2}[\exp(-b_1t)-\exp(-9b_1t)] \quad (68)$$

and

$$K_Q(t)=\sum_{n=0}^{\infty}\exp\left\{-\left[(2n+1)\frac{\pi}{2}\right]^2\frac{\nu}{H^2}t\right\}\doteq B\exp(-b_1t)$$

where $A=9\pi/32$, $B=\pi^2/8$, and $b_1=(\pi^2/4)(\nu/H^2)$. From (68), the alternate kernels follow

$$\sum_{n=0}^{\infty}\frac{(-1)^n}{\left[(2n+1)\frac{\pi}{2}\right]\frac{\nu}{H^2}}\exp\left\{-\left[(2n+1)\frac{\pi}{2}\right]^2\frac{\nu}{H^2}t\right\}\doteq A\frac{\pi}{2b_1}\left[\exp(-b_1t)-\frac{1}{9}\exp(-9b_1t)\right] \quad (69)$$

and

$$\sum_{n=0}^{\infty}\frac{1}{\left[(2n+1)\frac{\pi}{2}\right]^2\frac{\nu}{H^2}}\exp\left\{=\left[(2n+1)\frac{\pi}{2}\right]^2\frac{\nu}{H^2}t\right\}\doteq\frac{B}{b_1}\exp(-b_1t).$$

Then equation (67) can be written as

$$0=\mathrm{Re}\ (61)=\int_0^t\left\{\frac{A\pi}{2b_1}[{}^{(x)}F(t-\tau)\cos f\tau+{}^{(y)}F(t-\tau)\sin f\tau][e^{-b_1\tau}-e^{-9b_1\tau}]+\frac{B}{b_1}[{}^{(x)}Q(t-\tau)\cos f\tau+{}^{(y)}Q(t-\tau)\sin f\tau]e^{-b_1\tau}\right\}d\tau. \quad (70)$$

This may be written in convolution form as

$$0={}^{(x)}\mathcal{K}_F*{}^{(x)}F+{}^{(y)}\mathcal{K}_F*{}^{(y)}F+{}^{(x)}\mathcal{K}_Q*{}^{(x)}Q+{}^{(y)}\mathcal{K}_Q*{}^{(y)}Q \quad (71)$$

where

$${}^{(x)}\mathcal{K}_F=\frac{A\pi}{2b_1}\cos ft(e^{-b_1t}-e^{-9b_1t}),\ \ldots\ \text{etc.}$$

Then equation (71) implies

$${}^{(x)}\hat{Q}=-{}^{(x)}\hat{F}\frac{{}^{(x)}\hat{\mathcal{K}}_F}{{}^{(x)}\hat{\mathcal{K}}_Q}-{}^{(y)}\hat{F}\frac{{}^{(y)}\hat{\mathcal{K}}_F}{{}^{(x)}\hat{\mathcal{K}}_Q}-{}^{(y)}\hat{Q}\frac{{}^{(y)}\hat{\mathcal{K}}_Q}{{}^{(x)}\hat{\mathcal{K}}_Q} \quad (72)$$

where $\hat{(\ )}$ means $\hat{(\ )}=\int_0^{\infty}(\ )e^{-st}dt$. After some algebraic manipulation,

$$\frac{{}^{(x)}\hat{\mathcal{K}}_F}{{}^{(x)}\hat{\mathcal{K}}_Q}=1+b_1\frac{s^2+10b_1s+9b_1^2-f^2}{[s+b_1][(s+9b_1)^2+f^2]},$$

$$\frac{{}^{(y)}\hat{\mathcal{K}}_F}{{}^{(x)}\hat{\mathcal{K}}_Q}=\frac{9}{8}f\left[\frac{1}{(s+b_1)}-\frac{1}{9}\frac{s^2+2b_1s+b_1^2+f^2}{[s+b_1][(s+9b_1)^2+f^2]}\right], \quad (73)$$

and

$$\frac{{}^{(y)}\hat{\mathcal{K}}_Q}{{}^{(x)}\hat{\mathcal{K}}_Q}=\frac{f}{s+b_1}.$$

Applying the above to (72) and taking the inverse transform, one obtains

$${}^{(x)}Q(t)=-{}^{(x)}F(t)-\frac{b_1}{64b_1^2+f^2}\int_0^t{}^{(x)}F(t-\tau)[f^2e^{-b_1\tau}+(64b_1^2+2f^2)\cos f\tau e^{-9b_1\tau}+8b_1fe^{-9b_1\tau}\sin f\tau]d\tau-\frac{f}{8(64b_1^2+f^2)}\int_0^t{}^{(y)}F(t-\tau)\left[\{9(64b_1^2+f^2)-f^2\}\times e^{-9b_1\tau}-64b_1^2e^{-9b_1\tau}\cos f\tau-\frac{8b_1}{f}(64b_1^2+2f^2)e^{-9b_1\tau}\times\sin f\tau\right]d\tau-f\int_0^t{}^{(y)}Q(t-\tau)e^{-b_1\tau}d\tau. \quad (74)$$

If the above is used in computations, then recursive relations could be formulated as in the main report. The presence of ${}^{(y)}Q$ in the last term is a complication; however, the Coriolis coefficient reduces this term several orders of magnitude compared to others, so that it can be ignored. For the case $H\to 0$, it follows that

$$\lim_{H\to 0}[{}^{(x)}Q(t)=-{}^{(x)}F(t)-\frac{1}{9}\int_0^t[{}^{(x)}F(t-\tau)\cos f\tau-{}^{(y)}F(t-\tau)\sin f\tau]\delta(\tau)d\tau],$$

$$\delta(\tau)=\text{Dirac function, or }{}^{(x)}Q(t)=-\frac{10}{9}{}^{(x)}F(t). \quad (75)$$

This relation is different from that given by equation (28) in the main report, where the exact kernels K_F, K_Q were used. The boundary condition applies to the coastal surface gradients and not the coastal surges.

If the exact kernels are used, then the relation of ${}^{(x)}Q$ to ${}^{(x)}F$ on the boundary having finite depths is complicated. For simplification, a solution is given only for the special case of $0=(W_{drift}+W_{slope})$, that is, the total transport vanishes at the boundary. Using equations (56) and (60), we form the following:

$$\hat{F}\frac{H}{\nu\alpha}\frac{\sinh\alpha(1+z)}{\cosh\alpha}+\hat{Q}\frac{H}{\nu\alpha^2}\left[1-\frac{\cosh\alpha z}{\cosh\alpha}\right]=0,\ \alpha=\sqrt{\frac{if+s}{\nu/H^2}},$$

or

$$\hat{F}=-\hat{Q}\left[\frac{1}{2}\operatorname{csch}^2\frac{\alpha}{2}-\frac{1}{\alpha}\coth\frac{\alpha}{2}\right]. \tag{76}$$

Now let

$$\hat{K}_1=\frac{1}{2}\operatorname{csch}^2\frac{\alpha}{2}\text{ and }\hat{K}_2=-\frac{1}{\alpha}\coth\frac{\alpha}{2}. \tag{77}$$

Inverse transforms of the above, using residues, are

$$K_1(t)=2+\frac{4\nu}{H^2}\exp(-ift)\sum_{n=1}^{\infty}\exp\left(-4\pi^2n^2\frac{\nu}{H^2}t\right)\times\left[1+t\frac{8\nu}{H^2}\pi^2n^2\right]$$

and (78)

$$K_2(t)=-2-\frac{4\nu}{H^2}\exp(-if\tau)\sum_{n=1}^{\infty}\exp\left(-4\pi^2n^2\frac{\nu}{H^2}t\right).$$

Applying the above to equation (76) gives

$$F(t)=-Q(t)+\frac{32\nu^2}{H^4}\pi^2\sum_{n=1}^{\infty}n^2\times\int_0^t Q(t-\tau)\tau\exp(-if\tau)\exp\left(-4\pi^2n^2\frac{\nu}{H^2}\tau\right)d\tau. \tag{79}$$

The limit of the above as $H\to 0$ gives

$$Q(t)=-\frac{3}{2}F(t) \tag{80}$$

since

$$\int_0^{\infty}\frac{32\nu}{H^2}\pi^2\sum_{n=1}^{\infty}tn^2\exp\left(-4\pi^2n^2\frac{\nu}{H^2}t\right)dt=\frac{2}{\pi^2}\sum_{n=1}^{\infty}\frac{1}{n^2}=\frac{1}{3}.$$

This is another derivation of equation (28) in the main report.

APPENDIX D

In numerical computations with finite differencing, we use Shuman's (1962) notation:

$$\overline{U}_t^t=\frac{1}{2\Delta t}[U_{I,J}^{m+1}-U_{I,J}^{m-1}];\ \overline{U}^{xxyy}=\frac{1}{16}\begin{vmatrix}1&2&1\\2&4&2\\1&2&1\end{vmatrix}U_{I,J}^m; \tag{81}$$

$$\overline{U}_x^{xyy}=\frac{1}{8\Delta s}\begin{vmatrix}-1&0&1\\-2&0&2\\-1&0&1\end{vmatrix}U_{I,J}^m;\text{ and }\overline{U}_y^{xxy}=\frac{1}{8\Delta s}\begin{vmatrix}1&2&1\\0&0&0\\-1&-2&-1\end{vmatrix}U_{I,J}^m.$$

INTERIOR POINTS

The momentum prediction equations given by equation (4b) in finite-difference form are

$$\overline{U}_t^t=-gH_{I,J}\overline{h}_x^{xyy}+f\overline{V}^{xxyy}+\overline{\left[{}^{(x)}F+gH\frac{\partial h_0}{\partial x}-\sum_{j=1}^{3}\mathcal{C}(r_j)\right]}^{xxyy}$$

and (82)

$$\overline{V}_t^t=-gH_{I,J}\overline{h}_y^{xxy}-f\overline{U}^{xxyy}+\overline{\left[{}^{(y)}F+gH\frac{\partial h_0}{\partial y}-\sum_{j=1}^{3}\mathcal{C}(i_j)\right]}^{xxyy}.$$

The terms ${}^{(x)}F$, ${}^{(y)}F$, (gH) $(\partial h_0/\partial x)$, and $(gH)(\partial h_0/\partial y)$ are driving forces computed from the model storm; the derivative of the inverted barometric effect (atmospheric pressure gradient) is given and need not be set in finite-difference form. Equations (20) and (21) are used to evaluate $\Sigma\,\mathcal{C}(r_j)$, $\Sigma\,\mathcal{C}(i_j)$ at time $m\Delta t$. The dynamic surface slope gradients in (21) are not given, therefore they are set as $\overline{h}_x^{xyy}$, $\overline{h}_y^{xxy}$.

Empirical tests without the smoothing operator $\overline{(\ )}^{xxyy}$ gave small spurious waves in the basin in the vicinity of the storm center. This could be the result of the atmospheric pressure driving force (and other variables of the storm model) computed with an error of position as great as half a mile at grid points of the basin. The smoothing operator applied to the driving forces of the storm did damp out the small spurious waves, and for convenience in computations was also applied to the Coriolis and bottom stress terms. Except for the small spurious waves, the results were nearly the same with or without the smoothing operator.

The continuity equation (4) becomes

$$\overline{h}_t^t=-\overline{U}_x^{xyy}-\overline{V}_y^{xxy}. \tag{83}$$

OPEN BOUNDARIES

With open boundaries, it is impossible to use the nine-point difference forms of equation (81). The centered difference form $\overline{U}_x^x$ was used for gradients along the boundaries, and the uncentered form

$$\frac{\partial U}{\partial x}\simeq\frac{1}{2\Delta s}[-3U_{I,J}^m+4U_{I+1,J}^m-U_{I+2,J}^m] \tag{84}$$

was used for gradients normal to the boundary.

COASTAL BOUNDARY

The centered difference form is used to compute transport parallel to the coast. The boundary equation (24) is used to compute surges on the coast in preference to the continuity equation (4). To display the dynamic slope at the boundary, we rewrite the boundary equation with

the aid of (2) at the time $m\Delta t$ as

$$gH\frac{\partial h}{\partial x}=\left[fV+{}^{(x)}F-gH\frac{\partial h_0}{\partial x}-\sum_{j=2}^{3}\mathcal{C}^{m}_{(r_j)}-\left\{\mathcal{C}^{m}_{(r_1)}-\frac{2\nu}{H^2}E_{(r)1}gD\frac{\partial h}{\partial x}\right\}\right]\Big/\left[1-\frac{2\nu}{H^2}E_{(r)1}\right]. \quad (85)$$

In $\mathcal{C}^{m}_{(r_1)}$, there is a term containing $(\partial h/\partial y)^m$ which cannot be determined explicitly, but it is multiplied by a small coefficient and can be safely ignored or else replaced with known slopes at interior points. Iterative tests show that the coastal surge is insensitive to this term in the boundary equation. The term $(2\nu/H^2)$ $(E_{(r)1})$ in the divisor approaches 1 as $H\rightarrow 0$, which is readily seen by examining equation (14); therefore, zero depths cannot be used.

An extrapolation scheme is now used where surge heights on interior grid points of the basin are connected to the boundary in conformity with the slope given by the left side of equation (85); this is done using the uncentered difference form (84). Because the depths vary, the following identity is used

$$H\frac{\partial h}{\partial x}=\frac{\partial Hh}{\partial x}-h\frac{\partial H}{\partial x}. \quad (86)$$

Empirical tests show that the right side is preferable when using uncentered difference forms. For notational convenience, we denote the right side of (85) by $\mathcal{A}^{m}_{0,J}$ and use the right side of (86) with (84) to form

$$h^{m}_{0,J}=h^{m}_{boundary}=\left[\frac{2\Delta s}{g}\mathcal{A}^{m}_{0,J}+4H_{1,J}h^{m}_{1,J}-H_{2,J}h^{m}_{2,J}\right]\div[4H_{1,J}-H_{2,J}]. \quad (87)$$

Although analytic solutions satisfying the boundary equation (24) do satisfy continuity conditions on the boundary, there is no guarantee that the numerical scheme of this study satisfies continuity on the boundary. Stability studies for mixtures of centered, uncentered, and nine-point difference forms lie beyond the scope of this study. Empirical comparisons between computed and observed results are used as an indicator of the effectiveness of the numerical scheme.

ACKNOWLEDGMENTS

The author is sincerely grateful to Prof. Willard J. Pierson, Jr., for his invaluable guidance, criticism, and encouragement during the course of this investigation. Appreciation is also due Professors Gerhard Neumann, Albert D. Kirwan, Jr., and Richard M. Schotland for their many kind advices and helpful suggestions. Special thanks are expressed to Dr. Albion Taylor for the many friendly hours of conversation we spent together during the investigation as well as his critique and proofreading of the manuscript.

REFERENCES

Apostol, T., *Mathematical Analysis*, Addison-Wesley Publishing Co., Inc., Reading, Mass., **1967**, 552 pp. (see p. 459).

Dwight, Herbert B., *Tables of Integrals and Other Mathematical Data*, The Macmillan Co., New York, **1961**, 336 pp. (see p. 90).

Ekman, Vagn W., "On the Influence of the Earth's Rotation on Ocean Currents," *Archiv für Matematik, Astronomii, och Fysik*, Vol. 2, No. 11, K. Svenska Vetenskaps-akademien, Stockholm, **1905**, pp. 1–53.

Ekman, Vagn W., "Über Horizontalzirkulation bei Winderzeugten Meeresströmungen" (Concerning Horizontal Circulation in Connection with Wind-Generated Ocean Currents), *Archiv für Matematik, Astronomii, och Fysik*, Vol. 17, No. 26, K. Svenska Vetenskaps-akademien, Stockholm, **1923**, pp. 1–74.

Fjeldstad, Jonas E., "Ein Beitrag zur Theorie der Winderzeugten Meeresströmungen" (A Contribution to the Theory of Wind-Generated Ocean Currents), *Gerlands Beitrage zur geophysik*, Vol. 23, No. 3, Akademische verlagsgesellschaft M. B. H., Leipzig, **1929**, pp. 237–247.

Greenspan, H. P., "The Generation of Edge Waves on a Continental Shelf," *Journal of Fluid Mechanics*, Vol. 1, No. 6, Dec. **1956**, pp. 592–674.

Hansen, von Walter, "Theorie zur Errechnung des Wasserstandes der Stromungen in Randmeeren nebst Anwendungen" (Theory of Calculation of the Water Level and Currents in Marginal Seas, with Applications), *Tellus*, Vol. 8, No. 3, Aug. **1956**, pp. 287–300.

Harris, D. L., "Characteristics of the Hurricane Storm Surge," *Technical Paper* No. 48, U.S. Weather Bureau, Washington, D.C., **1963**, 139 pp.

Hidaka, Koji, "Non-Stationary Ocean Currents, Part I," *Memoirs of the Imperial Marine Observatory*, Vol. 5, No. 3, Kobe, Japan, **1933**, pp. 141–266.

Jelesnianski, Chester P., "Numerical Computations of Storm Surges Without Bottom Stress," *Monthly Weather Review*, Vol. 94, No. 6, June **1966**, pp. 379–394.

Jelesnianski, Chester P., "Numerical Computations of Storm Surges With Bottom Stress," *Monthly Weather Review*, Vol. 95, No. 11, Nov. **1967**, pp. 740–756.

Longuet-Higgins, M. S., "On the Trapping of Wave Energy Round Islands," *Journal of Fluid Mechanics*, Vol. 29, Part 4, Sept. **1967**, pp. 781–821.

Miyazaki, M., "Numerical Computations of the Storm Surge of Hurricane Carla 1961 in the Gulf of Mexico," *Ocean Magazine*, Vol. 17, Nos. 1–2, Nov. **1965**, pp. 109–140.

Munk, W. H., Snodgrass, F., and Carrier, G., "Edge Waves on a Continental Shelf," *Science*, Vol. 123, No. 3187, Jan. **1956**, pp. 127–132.

Neumann, G., and Pierson, W., Jr., *Principles of Physical Oceanography*, Prentice-Hall Publishing Co., Inc., New York, **1966**, 545 pp. (see p. 212).

Nomitsu, Takaharu, "A Theory of the Rising Stage of Drift Current in the Ocean: I. The Case of No Bottom Current," *Memoirs*, Ser. A., Vol. 16, No. 2, College of Science, Kyoto Imperial University, Japan, Mar. **1933***a*, pp. 161–175.

Nomitsu, Takaharu, "On the Development of the Slope Current and the Barometric Current in the Ocean: I. The Case of No Bottom Current," *Memoirs*, Ser. A., Vol. 16, No. 2, College of Science, Kyoto Imperial University, Japan, Mar. **1933***b*, pp. 203–242.

Platzman, George W., "The Dynamical Prediction of Wind Tides on Lake Erie," *Meteorological Monographs*, Vol. 4, No. 26, Sept. **1963**, 44 pp.

Reid, R. O., "Effect of Coriolis Force on Edge Waves: I. Investigation of the Normal Modes," *Journal of Marine Research*, Vol. 16, No. 2, **1958**, pp. 109–144.

Riesz, Frigyes, and Sz.-Nagy, B., *Functional Analysis*, Frederick Ungar Publishing Co., New York, **1955**, 468 pp. (see p. 37).

Shen, M. C., and Meyer, R. E., "Surface Wave Resonance on Continental and Island Slopes," *MRC Technical Summary Report* No. 781, Mathematics Research Center, University of Wisconsin, Madison, Sept. **1967**, 64 pp.

Shuman, Frederick, "Numerical Experiments With the Primitive Equations," *The Proceedings of the International Symposium on Numerical Weather Predictions, Tokyo, Japan, November* **7–13, 1960**, Meteorological Society of Japan, Tokyo, Mar. **1962** pp. 85–108.

Welander, P., "Wind Action on a Shallow Sea: Some Generalizations of Ekman's Theory," *Tellus*, Vol. 9, No. 1, Feb. **1957**, pp. 43–52.

[Received July 24, 1969; revised February 3, 1970]